Journal of Physics:
Conference Series

PAPER • **OPEN ACCESS**

Experimental Characterization of a Small-Scale PEM Water Electrolyzer for Hydrogen Production

To cite this article: Marco Russo Cirillo *et al* 2025 *J. Phys.: Conf. Ser.* **3143** 012078

Experimental Characterization of a Small-Scale PEM Water Electrolyzer for Hydrogen Production

Marco Russo Cirillo[1], Federico Del Mondo[1], Davide Pivetta[1], Damiano Perusi[2], Matteo Miola[2], Giovanna Marussi[3], Matteo Crosera[3], Luigi Migliorini[2], Marco Bogar[1] and Rodolfo Taccani[1*]

[1] Department of Engineering and Architecture, University of Trieste, Via Alfonso Valerio 6/1,34127, Trieste, Italy
[2] Enphos s.r.l., Via Zorzi 7, 37138 Verona, Italy; enphos@enphos.com
[3] Department of Chemical and Pharmaceutical Sciences, University of Trieste, Via Giorgeri 1, Trieste 34127, Italy

[*]E-mail: marco.russocirillo@phd.units.it

Abstract.

Proton Exchange Membrane water electrolyzer (PEMWEs) are expected to play a pivotal role in supporting the energy transition due to their efficiency and capabilities to handle dynamic loads, which makes them suitable for integration with renewable energy sources. This work presents experimental tests on a 2 kW PEM electrolyzer stack operating at 100kPa, with an active area of 28.3 cm*2* and 15 cells connected in series implemented at the University of Trieste Energy System Lab. The overall activity, carried out in collaboration with ENPHOS s.r.l., aims also to develop a test bench for the performance characterization of the stack and the balance of plant components. In this paper the authors focus on the description of the plant and the preliminary stack tests. The methodology to characterize the performance of the stack consists of a first polarization curve to assess the beginning of life performance, then start-stop cycles are applied to evaluate possible initial degradation of the performance detectable by polarization curve variations. The test rig results to be suitable to test the performance of the stack. The preliminary experimental data show the stack efficiency is 60% at low load (56 kWh/kg) and decreases to 40% at the maximum load (2 kWel). There was no appreciable degradation in terms of efficiency from the beginning and the end of the tests.

1. Introduction

The development of a wide hydrogen economy has recently seen a new growing interest as a key enabler for the reduction of greenhouse gas emissions within the so called hard-to-abate sectors. In fact, hydrogen, used as an energy vector can be exploited in transport sector like heavy duty

vehicle and ships, power generation system, in chemical industries, and can be used to store the surplus of energy production from intermittent renewable energy sources.

According to the Net Zero Emissions by 2050 Scenario (NZE Scenario) the global demand for hydrogen will increase of 50% by 2030 [1]. Nonetheless, in 2023 the global demand for hydrogen reached 97 million tons, which production was almost entirely sustained by non-renewable energy sources [1].

To date, the most widely hydrogen production process is steam methane reformation process, which is still the cheapest hydrogen production method currently available. Nonetheless, steam methane reforming cannot be considered a sustainable method of production as CO and CO_2 are produced during operation (10 kg_{CO2}/kg_{H2}) [2], and expensive purification methods are needed to be used in order to produce hydrogen with a satisfying degree of purity [3]. On contrary, green hydrogen production via electrolysis is characterised by absence of direct greenhouse gases emissions [4], as the electrical energy required to supply the energy needed for sustaining the water splitting reaction can be directly fed by renewable energy sources. Hence, to enhance the profitability of green hydrogen, reducing dependence on fossil fuels and avoid greenhouse gas emissions, it is crucial to improve the efficiency of this production process. To date, there are three technologies available on the market for green hydrogen production: Proton Exchange Membrane (PEM), alkaline and Solid Oxide. Despite higher costs, PEM water electrolysers allow to produce hydrogen with efficiencies in the order of 67-82 % [5], high degree of gas purity, and they are characterised by better capabilities to operate under variable loads (which are typical of renewable energy sources), making them a compelling solution for green hydrogen production [6] [7].

PEMWE cells are composed by an outer bipolar plate, one transport layer and one catalyst layer for each electrode. Electrodes are divided by a proton exchange membrane ensuring electrical insulation and sustaining proton transport from the anode to the cathode [8]. The catalytic layers (made of platinum/carbon at the cathode and iridium at the anode) are employed to foster redox reaction evolution at each electrode, while transport layers (carbon paper on the cathode and titanium porous on the anode) are used to facilitate the distribution along the whole surface of the electrode of electrical charge, reactant supply, and products of reaction drainage [9] [10] [11]. To sustain hydrogen production at industrial level, multiple cells are connected together to form a stack. Characterization of electrolyser stacks form the electrochemical point of view is not straightforward. Indeed, further research is required to fully comprehend the mechanism of degradation processes involving the electrochemical section as a function of the operating point and aging degree [12]. Consequently, there is an absence of effective standards for proper testing of electrolysers' operation under constant load, dynamic load cycling (e.g. photovoltaic energy profiles), or start-up/shut-down. Recently, however, several studies have been conducted on the behaviour of single cells under different load conditions [13] and specific photovoltaic profiles [14] and on-off cycles [15]. The complexity and costs of electrolysis plants has resulted in a limitation of studies that connect findings at a single cell level with the behaviour of electrolyser stacks.

In this framework, the capabilities of PEMWEs to operate under variable loads are investigated [16]. The present study provides a preliminary characterisation of a 2kW PEMWE, realised with the aim of further investigating the effects of different load conditions.

2. Materials and methodology

2.1 Plant description

The following work is addressing to characterise PEMWE stack of 2kW of nominal power (manufacturer qualified by Enphos s.r.l. [17]), which specifications are summarized in Table 1. The stack was hosted in a dedicated plant, as sketched by the Balance of Plant represented in Figure 1. The different sub-systems composing it can be divided by three distinct sections: water sub-system (in which process water is circulated within the electrolyser and from which hydrogen and oxygen are conveyed outside the circuit), cooling sub-system (where water-glycol coolant is employed for controlling the process fluid temperature), and refrigeration sub-system (using R449A as refrigerant, used to control the temperature of water-glycol solution).

Type I deionized water [18] was used as a process fluid, in agreement with the specifications provided by the supplier, to minimize contamination of the components MEA. A deionization water filter has been used to protect the stack from being poisoned by impurities and the degree of water purity is monitored by measuring water conductivity at the inlet of the electrolyzer. In this configuration, the water flows exclusively at the anode side, resulting in a single anode inlet and two outlets – anode and cathode – for the stack. The mixture of oxygen and water exiting the stack, enters into a condensateion column where the gaseous and liquid phases are separated, the

Table 1: Stack datasheet. Stack technical specifications provided by the manufacturer.

Specific	Unit	Value
Power	kW	2.0
Electrochemical active cell area	cm^2	28.3
Number of cells	-	15
Maximum operating temperature	°C	85
Minimum water flow rate	L/min	1.5
Operating voltage range	V	24.5 - 33.4
Operating current range	A	2.8 – 62.2
Hydrogen flow rate	L/min	6.50
Anode operating pressure	bar	1
Water conductivity	µS/cm	< 0.5
Maximum cathode operating pressure	bar	40
Maximum anode operating pressure	bar	1

water is then recirculated and oxygen is vented. Due to water drag and diffusion across the membrane and towards the cathodic electrodes, a mixture of hydrogen and water vapor which is found at the outlet of the stack requires to be processed to separate hydrogen from water vapor. Therefore, the gas mixture is fed into a chiller to be cooled down; a liquid phase separator is further used to separate produced gas from the condensed water. Recovered water obtained is recirculated back into the main tank. The refrigerant circuit is composed of a compressor, which conveys R449A refrigerant gas through the condenser. In this process, the gas undergoes a lamination process which leads to a reduction in temperature which is useful for chilling the coolant. The sensors employed within the plant for monitoring purposes are listed in Table 2.

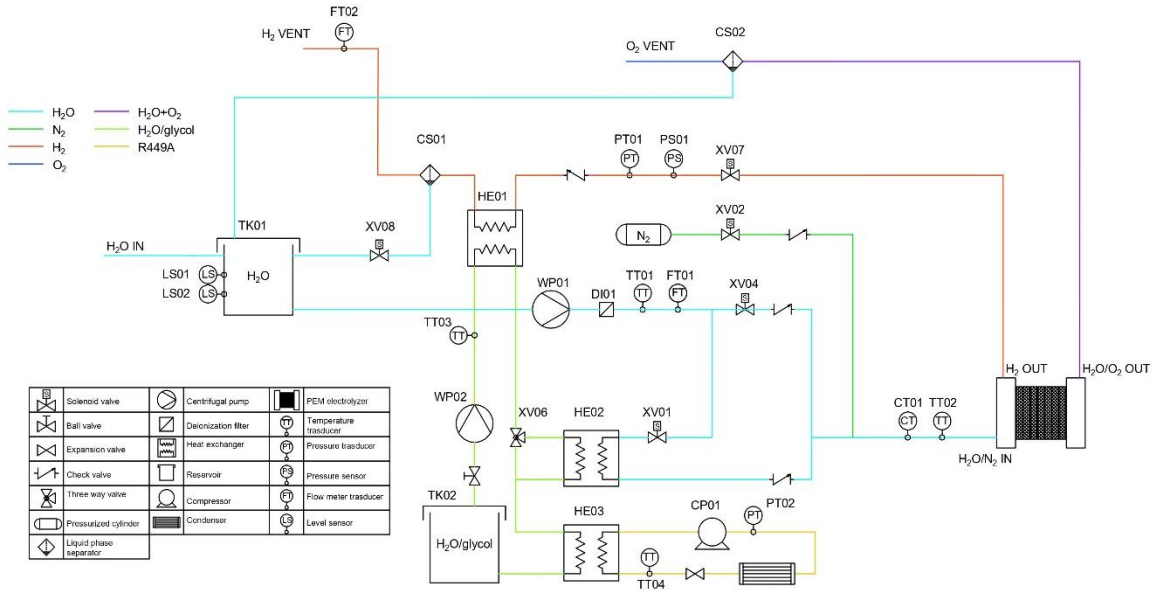

Figure 1: Plant layout. Piping and Instrumentation Diagram (P&ID) of the entire plant.

Table 2: Sensors. List of the sensors implemented in the plant. Voltage was directly measured between the stack bipolar plates.

P&ID element	Sensor type	Manufacturer / model
FT02	Hydrogen flow rate	Bronkhorst / F-201CV
FT01	Water flow rate	IFM / SV4050
TT01 to TT04	Temperature	- / 1 kΩ NTC
CT01	Conductivity	Supmea / SUP–TDS210-B; probe: K = 0.01
-	Current sensor	Seneca / TS201DCH100

2.2 Testing procedure

The stack has been characterised in agreement with the guidelines proposed by the Joint Research Centre (JRC), introducing the techniques for cells and small stacks stress tests. This study refers to the test protocol 8.4.6 (Cold start time to nominal power test protocol) of the EU harmonized protocols for testing of low temperature water electrolysers guideline [19] and the following stack-on/off procedures visualized in Figure 2:

- During the *start-up* phase, a current of 2.8 A (corresponding to 0.1 A/cm^2) is applied for a duration of five minutes. Subsequently, a current ramp (slope: 0.1 A/s) brings the current to its maximum value (60 A, 2.1 A/cm2), until the operating temperature of 70°C degrees is reached.
- Stack working point is *maintained* constant for 15 minutes. This enables the stability of the process parameters to be monitored and recorded.
- Subsequent *shut-down* consists of a ramp of decreasing current (slope: 0.1 A/s), which is run until the null current.

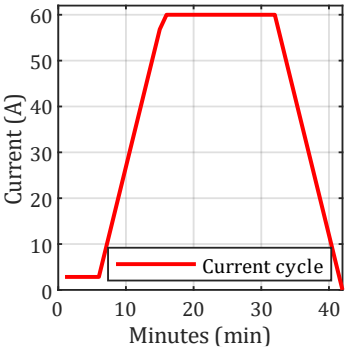

Figure 2: Current cycle. Current variation during the on/off cycle.

In between consecutive cycles, a cooling step is run until temperature of process water returns below 30°C degrees. This step is implemented by circulating water in the heat exchanger where it is cooled down by the water-glycol subsystem before it enters the stack. The analysis considers 50 start-up/shut-down cycles and the electrolyzer has been operated with a water flow rate of 5.51 ± 0.05 sL/min, and a cathode and anode pressure of 100 kPa.

To compare evolution of stack performances, polarization curves were recorded periodically at the temperature of 70°C, in accordance with the guidelines issued by the Joint Research Centre [20] (starting from 0.018 A/cm^2 to 2.148 A/cm^2 with step of 0.035 A/cm^2 and right after, a downward curve with the same steps). Stack performances have been recorded every 5 cycles and compared with the performances recorded at initial conditions (Beginning of Life, BOL).

2.3 Inductively Coupled Plasma-Mass Spectrometry (ICP-MS)

In order to monitor the possible dissolution of iridium, 15 mL of process water were collected every five cycles before polarization curve recording. An Inductively Coupled Plasma Mass Spectrometry (ICP-MS) with a NexION 350X instrument (PerkinElmer, USA), equipped with an ESI SC Autosampler was used for searching for traces of Ir and Ti. To reduce polyatomic ion interferences originating in the plasma, analyses were performed in Kinetic Energy Discrimination (KED) mode with a high-purity helium gas flow rate of 4.8 mL·min-1. Instrument calibration was achieved using a series of standard solutions ranging from 0.2 to 100 µg·L^{-1}, obtained through serial dilution of 10 mg·L^{-1} multielement standards designed for ICP applications (Periodic Table MIX 1 and MIX 2, TraceCERT, Sigma-Aldrich). Quantification of analytes was based on a linear calibration curve within the specified concentration range (0.2–100 µg·L^{-1}, R_2 = 0.99).

Analytical accuracy was verified using two quality control samples at concentrations of 1 µg·L^{-1} and 10 µg·L^{-1}, prepared from a separate multielement standard not employed in calibration

(Multielement Quality Control Standard for ICP, VWR Chemicals). The limits of detection (LOD) for each Ir (193 u.m.a.) and Ti (48 u.m.a.) were equal to 0.05 μg·L^{-1} and 0.1 μg·L^{-1}, respectively. Measurement precision as repeatability (RSD%) for the analysis was < 3%.

2.4 Data acquisition and performance evaluation

Data processing and automation has been performed via LabVIEW (National Instruments). The main parameters of the plant (water temperature, water flow rate, hydrogen flow rate $\dot{m}_{H_2}$, voltage of the stack V_{stack}, applied current I) has been recorded at the frequency of 1 Hz. From recorded data, stack efficiencies and its specific consumption are calculated.
Stack efficiency was calculated as a ratio among the product of the mass flow rate of hydrogen produced by the electrolyzer ($\dot{m}_{H_2}$) and the hydrogen lower heating value (120 MJ/kg) over the electrical power supplied to the stack (P_{tot}) [21] [22].

$$\eta_{stack} = \frac{\dot{m}_{H_2} \cdot LHV}{P_{tot}} \tag{1}$$

For more detailed analysis, the overall efficiency was also evaluated in terms of voltage efficiency (ε_{vol},) and Faradaic efficiency (ε_{curr}), calculated as it follows [21]:

$$\varepsilon_{vol} = \frac{V_{rev}}{V_{stack}/N_{cell}} \tag{2}$$

$$\varepsilon_{curr} = \frac{2F \cdot \dot{m}_{H_2}}{N_{cell} \cdot I} \tag{3}$$

where V_{rev} is the reversible voltage (1.23V in standard condition), N_{cell} is the number of cells, and F is the Faraday constant $F = 96485\ C/mol$. Finally, the specific energy consumption is calculated according to:

$$\varepsilon_{cons} = \frac{V_{stack} \cdot I}{\dot{m}_{H_2}} \tag{4}$$

3. Results

The stack was characterized at first in pristine conditions by recording the polarization curve shown in Figure 3. After the first, sudden in proof of voltage due to activation losses characterizing the regime of low current density values, the voltage rises following a linear trend indicating that no mass transport limitations are occurring, and that ohmic losses are the most dominant contribution to the outlook of the polarization curve. Moreover, a comparison of the polarization curves recorded by sequentially applying a positive ramp and a negative ramp in Figure 3 reveals the absence of obvious hysteresis phenomena, thereby indicating that the system is operating within thermodynamic equilibrium conditions [20].

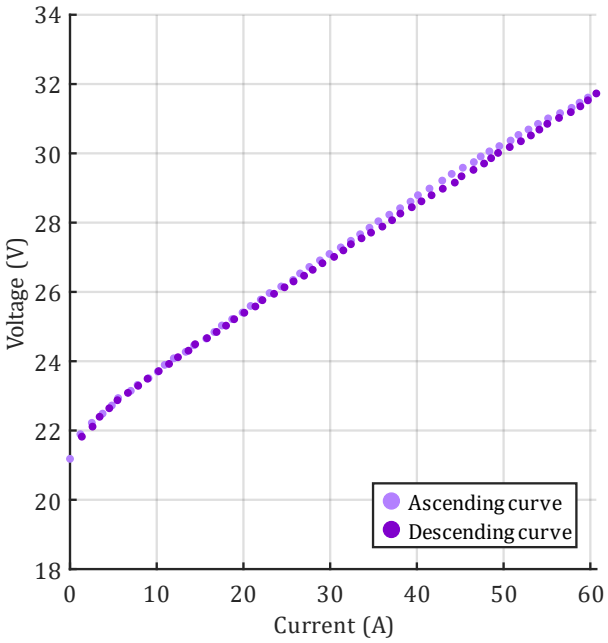

Figure 3: Polarization curve. Polarization curves recorded at 70°C differentiating the first positive upward curve and then the second downward curve.

Afterwards, the performances of the stack were characterized at stationary conditions, at 70 °C at nominal power of operation (1.96 kW): hydrogen production rate was measured to be 5.51 ± 0.05 sL/min at 61.6 A and 31.8V. Recorded performances are compared with data provided by the supplier in Table 3. As listed, measured efficiency deviates from the specifications provided by the manufacturer, with current efficiency exhibiting the most significant discrepancy. This can be related to some non-optimal separation among the hydrogen and water vapor. In addition, the higher value found of the specific consumption can be primarily attributed to the reduced amount of hydrogen measured at the system outlet in comparison to the manufacturer's stated data (6,50 sL/min).

In order to complete the analysis on these parameters, the following section will present an evaluation of the trend of these parameters during a mid-test polarization curve after 30 cycles in order to assess their variation with the applied current.

The two graphs in Figure 4 illustrate the operation of the PEM electrolyzer at varying load levels. As illustrated in Figure 4a, voltage efficiency exhibits a downward trend, with its

Table3: Efficiency comparison. All four efficiency parameters are calculated with both with the datasheet parameters and the parameters measured at the nominal power of 1.96kW

	η_{stack} (%)	ε_{vol} (%)	ε_{curr} (%)	ε_{cons} (kWh/kg)
Provided by the manufacturer	45.3	55.2	81.9	72.9
Measured	40.8	58.2	69.8	81.7

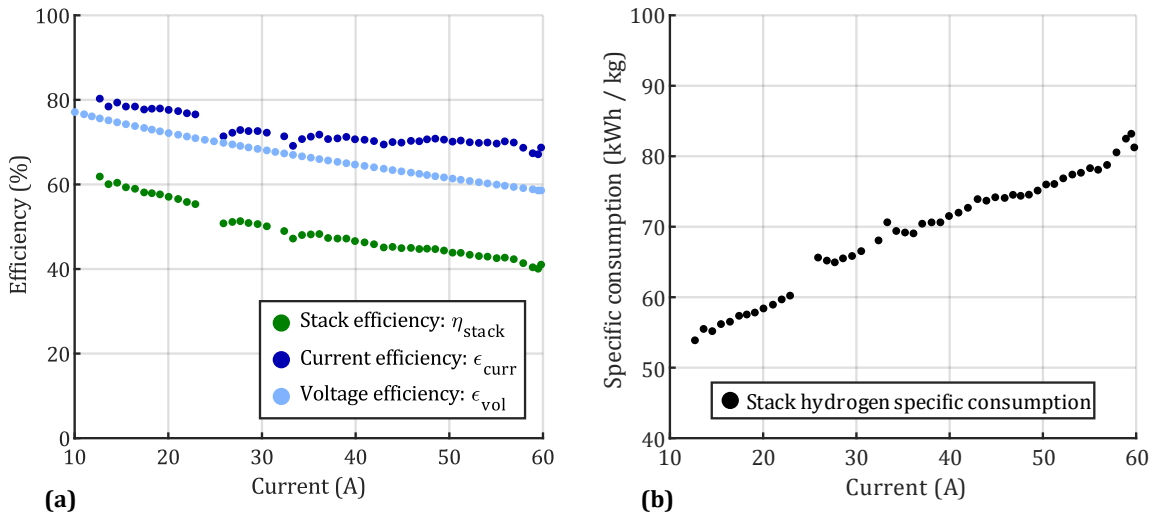

Figure 4: Efficiency of the stack. PEM stack performance evaluation at different current. (a) Efficiencies, (b) Hydrogen specific consumption

dependence on the recorded voltage values being the sole contributing factor. Subsequently, from the maximum initial level around 10 A, the two efficiencies demonstrate a downward trend, reaching the final values at maximum load reported previously in Table 3. It has been demonstrated that the electrolyzer exhibits optimal functionality at an output exceeding 10 A, attaining a global stack efficiency of 60% and a specific consumption around 55 kWh/kg. These values are in line with what is already reported in literature [23].

As previously explained, one of the purposes of this work is the preliminary assessment of the effect of start and stop cycles over stack performance, hence Figure 5 presents the evolution of polarization curves taken at a temperature of 70°C every 5 cycles.

It is evident that the polarization curves obtained show consistency in the relationship between voltage and current with a minimal deviation more visible at higher current densities (Figure 5b). Comparing the voltage evolution at fixed operating points (selected at 5, 30, and 60 A, corresponding to 0.18, 1.06, and 2.12 A/cm^2) in function of the cycle number of the stress-test cycle applied, depending on the operating point, the standard deviation from the average value was found equal to 0.07 V at low current values (5 A), 0.15 V at intermediate current values (30 A), and 0.20 V at high current values (60 A), leading to a final variation after 50 cycles equal to the 0.06%, 0.74%, and 1.22%, with respect initial conditions. Such variations are still little to underline the presence of any possible degradation phenomena. Nonetheless, ICP-MS revealed

losses of titanium equal to 0.70, 0.45, and 0.60 μg·L^{-1} after 30, 40, and 50 cycles respectively; more extended tests should be required.

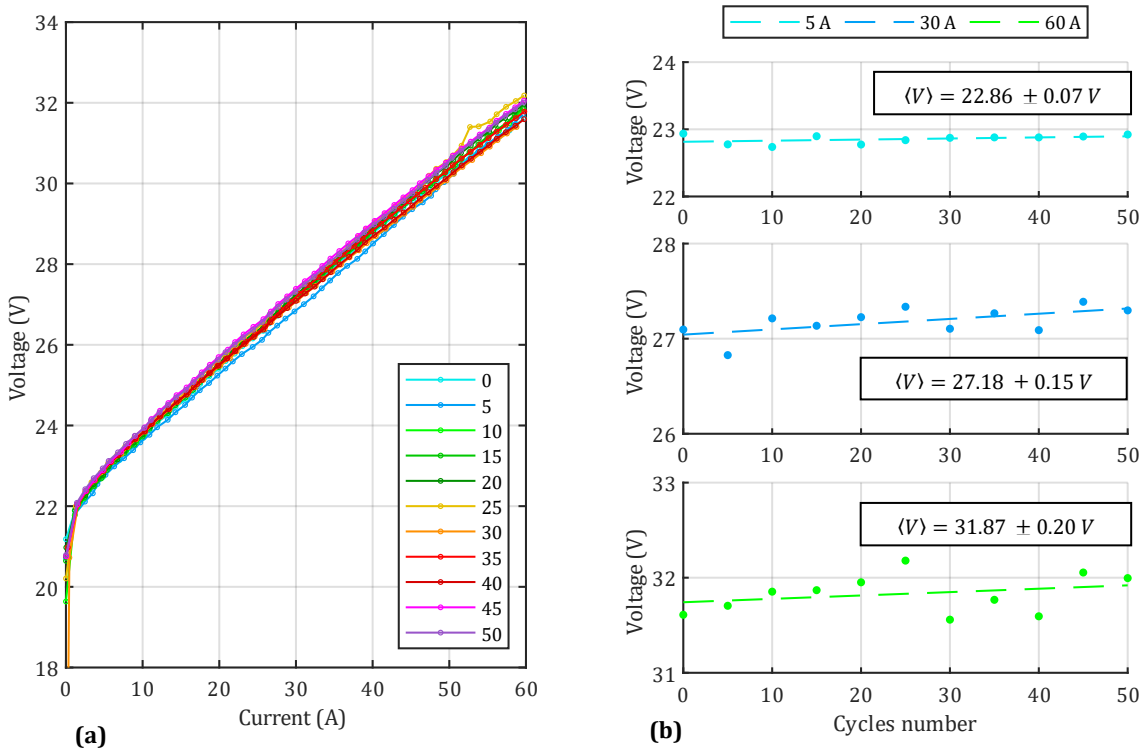

Figure 5: Performance evaluation over accelerated stress tests. (a) Time-resolve evolution of polarization curves during start-up/shut-down cycles displayed in function of the 50 cycles. (b) Evolution of the recorded stack voltage at specific current values (top: 5A, middle: 30A, bottom: 60A). Note: dashed line represents a guide for the eye only, the box within the graphs shows the average voltage value with the standard deviation.

4. Conclusion

In this work, the authors presented a test bench for electrolyzer performance assessment and a preliminary characterization of a prototypal PEM stack undergoing start-stop cycling. During the test the plant was found to be suitable to measure the performance of the stack and to simulate a real-life operating strategy. The preliminary accelerated stress test considering the start-stop cycles shows that after 50 cycles it was not possible to observe any significant degradation. The efficiency values obtained demonstrate stability in response to load variation, with a maximum value of 60% observed at 15% of the nominal power and an efficiency of 40% at full load. Thereby, specific consumption exhibits an increase from 55 to 80 kWh/kg, while operating at higher hydrogen production rate. Future analysis will address the stability over longer cycling periods to highlight the presence of degradation in the stack.

References

[1] IEA, “Global Hydrogen Review,” Paris, 2024.

[2] A. Ajanovic, M. Sayer and R. Haas, “On the future relevance of green hydrogen in Europe,” *Applied Energy,* 2024.

[3] L. Szablowski, M. Wojcik and O. Dybinski, “Review of steam methane reforming as a method of hydrogen production,” *Energy,* vol. 316, 2025.

[4] The Royal Society, “The role of hydrogen and ammonia in meeting the net zero challenge,” 2021.

[5] T. Wang, X. Cao and L. Jiao, “PEM water electrolysis for hydrogen production: fundamentals, advances, and prospects,” *Carbon Neutrality,* vol. 1, no. 1, p. 21, 2022.

[6] Fuel Cells and Hydrogen 2 Joint Undertaking, “Hydrogen Roadmap Europe: A sustainable pathway for the European Energy Transition,” Publications Office of the European Union, Bietlot, Belgium, 2019.

[7] Clean Hydrogen Joint Undertaking, “Strategic Research and Innovation Agenda 2021-2027,” Pubblications Office of the European Union, 2022.

[8] M. Carmo, D. L. Fritz, J. Mergel and D. Stolten, “A comprehensive review on PEM water electrolysis,” *International Journal of Hydrogen Energy,* vol. 38, no. 12, pp. 4901-4934, 2013.

[9] E. Kuhnert, V. Hacker and M. Bodner, “A Review of Accelerated Stress Tests for Enhancing MEA Durability in PEM Water Electrolysis Cells,” *International Journal of Energy Research,* vol. 2023, pp. 1-23, 2023.

[10] S. Shiva Kumar and V. Himabindu, “Hydrogen production by PEM water electrolysis - A review,” *Materials Science for Energy Technologies,* vol. 2, no. 3, pp. 442-454, 2019.

[11] P. Shirvanian and v. B. Frans, “Novel components in Proton Exchange Membrane (PEM) Water Electrolyzers (PEMWE): Status, challenges and fture needs. A mini review,” *Electrochemistry Communications,* vol. 114, 2020.

[12] E. Wallnöfer-Ogris, I. Grimmer , M. Ranz, M. Höglinger, S. Kartusch, J. Rauh, M.-G. Macherhammer, B. Grabner and A. Trattner, “A review on understanding and identifying degradation mechanism in PEM water electrolysis cells: Insights for stack application, development, and research,” *International Journal of Hydrogen Energy,* vol. 65, pp. 381-397, 2024.

[13] S. M. Alia, S. Stariha and R. L. Borup, “Electrolyzer Durability at Low Catalyst Loading and with Dynamic Operation,” *Journal of The Electrochemical Society,* vol. 166, pp. 1164-1172, 2019.

[14] E. Kuhnert, K. Mayer, M. Heidinger, C. Rienessel, V. Hacker and M. Bodner, “Impact of intermittent operation on photovoltaic-PEM electrolyzer systems: A degradation study based on accelerated stress testing,” *International Journal of Hydrogen Energy,* vol. 55, pp. 683-695, 2024.

[15] A. Weiß, A. Siebel, M. Bernt, T.-H. Shen, V. Tileli and H. A. Gasteiger, “Impact of Intermittent Operation on Lifetime and Performance of a PEM Water Electrolyzer,” *Journal of Electrochemical Society,* vol. 166, pp. 487-497, 2019.

[16] Q. Feng, X.-Z. Yuan, G. Liu, B. Wei, Z. Zhang, H. Li and H. Wang, "A review of proton exchange membrane water electrolysis on degradation mechanism and mitigation strategies," *Journal of Power Sources,* vol. 366, pp. 33-55, 2017.

[17] [Online]. Available: https://www.enphos.com. [Accessed 15 June 2025].

[18] ASTM D1193-99e1, *Standard Specification for Reagent Water,* 2017.

[19] G. Tsotridis and A. Pilenga , "EU harmonized protocols for testing of low temperature water electrolysers," Pubblications Office of the European Union, Luxembourg, 2021.

[20] T. Malkow, A. Pilenga , G. Tsotridis and G. De Marco, "EU harmonised polarisation curve test method for low-temperature water electrolysis," Pubblications Office of the European Union, Luxembourg, 2018.

[21] G. Tsotridis and A. Pilenga, "EU harmonised terminology for low-temperature water electroysis for energy-storage applications," Publications Office of the European Union, Luxembourg, 2018.

[22] T. Malkow and A. Pilenga, "EU harmonised testing procedure: Determination of water electrolyser energy performance," Publications Office of the European Union, Luxembourg, 2023.

[23] A. Buttler and H. Spliethoff, "Current status of water electrolysis for energy storage, grid balancing and sector coupling via power-to-gas and power-to-liquids: A review," *Renewable and Sustainable Energy Reviews,* vol. 82, no. 3, pp. 2440-2454, 2018.